10
Theory of Excitons in Carbon Nanotubes

In the resonance Raman spectroscopy of single-wall carbon nanotubes (SWNTs), the optical transition energy from the ith valence band state to the ith conduction band state, E_{ii}, is important for assigning (n, m) values to individual SWNTs. To assign the experimentally observed E_{ii} in single-wall carbon nanotubes, a theoretical development has been carried out with respect to the simple (nearest neighbor) tight-binding (STB) model discussed in Chapter 2. By adjusting the STB (simple tight-binding) parameters, E_{ii} values have been assigned to specific (n, m) SWNTs for a limited region of diameter or energy on the Kataura plot. However, this procedure is not useful for explaining in a systematic way the results obtained from many SWNT samples synthesized by different methods. In this chapter we discuss three aspects going beyond the STB model that are necessary to achieve experimental accuracy:

- Curvature (σ–π hybridization) effects using the extended tight-binding method;
- Excitonic effects using the Bethe–Salpeter equation;
- Dielectric screening effects of excitons.

This chapter begins with a brief description of how curvature effects are introduced into the tight-binding model, to construct what has been called the extended tight-binding (ETB) method (Section 10.1). The curvature effect in SWNTs is responsible for $\sigma - \pi$ hybridization, resulting in a much stronger E_{ii} dependence on the SWNT chiral angle θ than that predicted by the STB picture. In sequence, Section 10.2 gives a broad overview of exciton physics, which is the main part of this chapter. The electron–electron and the electron–hole interactions, generally called many-body effects, change in a significant way the E_{ii} dependence on tube diameter d_t, as well as the relative distance between the different E_{ii} levels. From a theoretical point of view, the importance of excitons to SWNTs was introduced early on by Ando [319], who studied the electronic excitations of nanotubes within a static screened Hartree–Fock approximation. Later on, after experimental results started to show the importance of excitons, detailed first-principles calculations of the effects of many-body interactions on the optical properties were performed for nanotubes with very small diameter [320–323] and some descriptions of excitons in nanotubes based on simpler models [324–327] were also developed.

Raman Spectroscopy in Graphene Related Systems. Ado Jorio, Riichiro Saito, Gene Dresselhaus, and Mildred S. Dresselhaus

ISBN: 978-3-527-40811-5

Following this work, a systematic dependence of exciton effects (including wave function-related phenomena) on the nanotube diameter and chiral angle was developed [186, 328, 329] and this topic is presented in Section 10.4.1. These results are important for providing a quantitative description of the photophysical properties of SWNTs, including the Raman response. Finally, Section 10.5 introduces the importance of the dielectric screening of an exciton by other electrons and by surrounding materials, a topic that is still under development in the science of one-dimensional systems.

10.1 The Extended Tight-Binding Method: σ–π Hybridization

The nearest neighbor (simple) tight-binding (STB) model, developed in Chapter 2, gives the first approximation in constructing a Kataura plot showing the dependence of the transition energies E_{ii} on the tube diameter d_t (Section 2.3.4). The several E_{ii} levels for SWNTs are shown in Figure 2.22 to exhibit a strong $1/d_t$ dependence, that is related to the distance of the cutting line from the K point in the unfolded 2D-graphene Brillouin zone, and there is in addition a small chiral angle θ dependence related to the trigonal warping effect [31]. However, the experimental results of E_{ii} as a function of d_t show from the observed $1/d_t$ dependence of E_{ii} for SWNTs (see Section 9.3.2) that the chirality-dependent pattern (family pattern) which occurs for (n, m) SWNTs with $(2n + m) =$ constant, is actually much larger than that predicted from the STB model. This experimental observation led to the implementation of the ETB model for the explanation of many experimental studies of the photophysics of SWNTs. This $(2n + m)$ spread is mainly attributed to the SWNT curvature effects, which cause a chiral angle dependence in the C–C bond length relaxation in small d_t SWNTs that is missing from the STB approximation.

It had been shown that long-range interactions of the p orbitals are not negligible [330], and the curvature of the SWNT sidewalls results in an important sp^2–sp^3 rehybridization in the small d_t limit. The curvature effect can be included in the tight-binding (TB) model [182, 329] by extending the basis set to the atomic s, p_x, p_y, and p_z orbitals that form the s and p molecular orbitals according to the formalism developed in Chapter 2 (the Slater–Koster formalism [31, 331]). This extended tight-binding (ETB) model utilizes the TB transfer and overlap integrals as a function of the C–C inter-atomic distance calculated within the density functional theory (DFT) framework [263], thus including long-range interactions and bond-length variations within the SWNT sidewall. The atomic p-orbitals are aligned with the cylindrical coordinates of the SWNT sidewall according to a symmetry-adapted scheme [182, 329] in which p_z is orthogonal to the SWNT sidewall, while p_x and p_y are parallel to the SWNT sidewall for each C atom. This choice allows us to consider an 8×8 Hamiltonian for the graphene unit cell of two C atoms (A and B), even for chiral SWNTs with large translational unit cells, thus greatly simplifying the calculations. Further details of the calculational method can be found in [329].

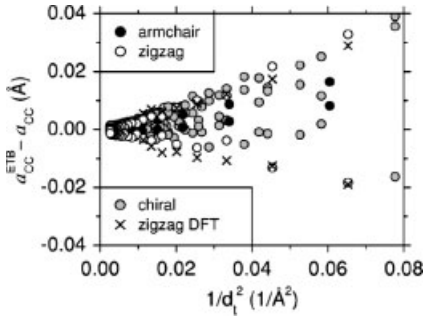

Figure 10.1 Differences between the C–C bond lengths a_{C-C} in the ETB model (denoted by a_{C-C}^{ETB}) and $a_{C-C} = 0.142$ nm in the flat graphene layer for many SWNTs as a function of nanotube curvature $1/d_t^2$. Open, closed, and gray dots denote the bond lengths of zigzag, armchair, and chiral SWNTs, respectively, calculated from the ETB model for the optimized SWNT structures. For comparison, crosses show the bond lengths of zigzag SWNTs from DFT calculations [182].

The total energy of the SWNT can be calculated using the short-range repulsive potential obtained from DFT calculations [263], and the geometrical structure optimization can then be performed. To compare the SWNT structures optimized by using the ETB model with the results of other independent geometrical structure optimizations, we plot in Figure 10.1 the change in the C–C bond lengths for each SWNT as a function of nanotube curvature $1/d_t^2$ [182]. For calculating the electronic structure of SWNTs, it is essential to utilize the optimized SWNT structure, since the overlap integrals are very sensitive to the relaxed atomic positions. As a consequence, the θ dependence (i. e., the family pattern in the Kataura plot) increases significantly with decreasing d_t, thereby matching the results observed in the experimental Kataura plot (Section 9.3.2).

10.2
Overview on the Excitonic Effect

The exciton is a bounded electron–hole pair. An exciton in a semiconducting material consists of a photoexcited electron and a hole bound to each other by an attractive Coulomb interaction. In many commonly occurring bulk 3D semiconductors (such as Si, Ge and III–V compounds), the binding energy of an exciton can be calculated by a hydrogenic model with a reduced effective mass and a dielectric constant, giving a binding energy on the order of $\sim$ 10 meV with discrete energy levels lying below the single particle excitation spectra. Thus optical absorption to exciton levels is usually observed only at low temperatures. However, in a single-wall carbon nanotube, because of its 1D properties, the electron–hole binding energy becomes much larger (and can be as large as 1 eV), so that exciton effects can be observed even at room temperature. Thus excitons are essential for

explaining optical processes, such as optical absorption, photoluminescence, and resonance Raman spectroscopy in SWNTs.

The following sections presents a broad descriptive picture of the theoretical description of excitons in SWNTs. It starts by briefly addressing the general properties of excitons in general, while also emphasizing the uniqueness of excitons in graphite, SWNTs and C_{60} and the difference in behavior between the excitons in each dimension (2, 1, and 0, as represented by these carbon materials, respectively.) The unusual geometrical structure of sp^2 carbons to which all of these materials relate gives rise to the two special points in the Brillouin zone (K and K'), which are related to one another by time reversal symmetry [80], making these sp^2 carbon systems unique relative to other nanosystems which also have large excitonic effects, but do not have similar symmetry constraints. Differences in symmetry are important and guide electronic structure calculations and the interpretation of experiments. Therefore, an analysis of exciton symmetries in SWNTs is needed to understand in greater detail many aspects of their optical properties, and this is the next topic of this section (Section 10.3). From the group theory analysis, the selection rules for optical phenomena in SWNTs are obtained (and are discussed in Section 10.3.2). Finally, Section 10.4 develops the theory for excitons in carbon nanotubes.

10.2.1
The Hydrogenic Exciton

The simplest treatment for an exciton is given by the Wannier exciton, which can be described by the Schrödinger equation:

$$\left[-\frac{\hbar}{2m_e^*}\nabla_e^2 - \frac{\hbar}{2m_h^*}\nabla_h^2 - \frac{e^2}{\epsilon r}\right]\Psi_{ex} = E_{ex}\Psi_{ex}\,, \tag{10.1}$$

where subscripts e, h stand for the electron and the hole of the exciton which are attracted by a Coulomb potential[1] $-e^2/\epsilon r$ (ϵ is the dielectric constant), and m_e and m_h are the effective mass of the electron and the hole, respectively. By adopting the center of mass coordinate $\boldsymbol{R} = (m_e\boldsymbol{r}_e + m_h\boldsymbol{r}_h)/(m_e + m_h)$ and the relative distance coordinate $\boldsymbol{r} = (\boldsymbol{r}_e - \boldsymbol{r}_h)$, the exciton wavefunction can be given by:

$$\Psi(\boldsymbol{R}, \boldsymbol{r}) = g(\boldsymbol{R})\, f(\boldsymbol{r})\,, \tag{10.2}$$

where $g(\boldsymbol{R}) = e^{i\boldsymbol{K}\cdot\boldsymbol{R}}$ describes the movement of an exciton with momentum $\boldsymbol{K}$, and $f(\mathbf{r})$ gives the different exciton levels with solutions obtained by the Schrödinger equation for a hydrogen atom with a reduced mass

$$\frac{1}{\mu} = \left(\frac{1}{m_h^*} + \frac{1}{m_e^*}\right)\,. \tag{10.3}$$

1) In SI (MKS) units, a Coulomb potential becomes $-e^2/4\pi\epsilon_0\epsilon r$. For a conversion from CGS to MKS units, we include a factor of $1/4\pi\epsilon_0$ along with e^2.

The solution of Eq. (10.1) gives:

$$E(\boldsymbol{K}) = -\frac{\mu e^4}{2\hbar^2 \epsilon^2 n^2} + \frac{\hbar^2 K^2}{2(m_e^* + m_h^*)}, \quad (n = 1, 2, 3, \ldots) . \tag{10.4}$$

The first and second terms in Eq. (10.4) are the excitonic energy levels denoted by the quantum number n and the energy dispersion relation for the center of mass motion of the exciton, respectively. Although the description of excitons in SWNTs is more complex, since the exciton is formed by the mixing of different k states due to the Coulomb interaction (as described below in Section 10.4), the concepts of a dispersion relation, exciton wave vector and excitonic energy levels are closely related to this simplified description.

10.2.2
The Exciton Wave Vector

A single-particle picture of carriers is simple and easy to understand. In a semiconducting material, an electron can be excited from the valence band to the conduction energy band, and the photon energy beyond the band gap goes into the kinetic energy of the excited electron. An excitonic picture, however, cannot be represented by a single-particle model, and we cannot generally use the energy dispersion relations directly to obtain the excitation energy for the exciton. If the electron and hole wavefunctions are localized in the same spatial region, the attractive Coulomb interaction between the electron and hole increases the binding energy, while the kinetic energy and the Coulomb repulsion between the electrons becomes large, too. Thus the optimum localized distances between the e–h (electron–hole) pair determine the exciton binding energy. In the case of a metal, the dielectric screening of the Coulomb interaction by other conduction electrons reduces the Coulomb interaction significantly (where ϵ is infinity) and thus the exciton does not form.[2)] The repulsive Coulomb interaction between a photoexcited electron and valence electrons causes the wave vector k for the excited electron to no longer be a good quantum number, since electron–electron scattering occurs and thus the lifetime of an electron becomes finite.

Since the exciton wavefunction is localized in real space, the exciton wavefunction in k space is a linear combination of Bloch wavefunctions with different k states. Thus the definition of k_c and k_v is given by their central values with a width of Δk.[3)]

When we consider an optical transition in a crystal, we expect a vertical transition, $k_c = k_v$ (Figure 10.2a), where k_c and k_v are, respectively, the wave vectors of the electron and the hole. The wave vector of the center of mass for the exciton is defined by $K = (k_c - k_v)/2$, while the relative coordinate is defined by $k = k_c + k_v$. Here, we note that the hole (created by exciting an electron) has the opposite sign for its wave vector and effective mass as compared to the electron. The exciton has

2) Metallic SWNTs have shallow exciton bound states relative to those for semiconducting SWNTs.
3) The Fourier transformation of a Gaussian in real space is a Gaussian in k space, too.

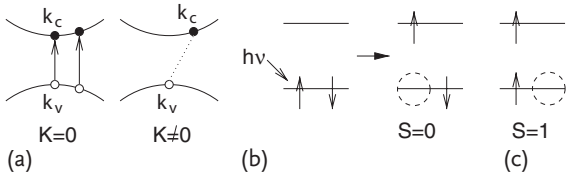

Figure 10.2 (a) A singlet exciton formed at $K = 0$ in a crystal where $k_c = k_v$ (left), at either the band extrema or away from the band extrema if $k_c \neq k_v$, $K \neq 0$, giving rise to a dark exciton (right, see text). (b) When a photon is absorbed by an electron with spin ↑ (left), we get a singlet exciton ($S = 0$, right). If the spin of the electron is ↑ we here define the spin of the hole that is left behind as ↓. (c) A triplet exciton ($S = 1$), that is a dark exciton [187].

an energy dispersion as a function of K, which represents the translational motion of an exciton. Thus only the $K = 0$ ($K < \Delta k$) exciton can recombine by emitting a photon. Correspondingly, a $K \neq 0$ exciton cannot recombine directly to emit a photon and therefore is a dark exciton. Recombination emission for $K \neq 0$ is, however, possible by a phonon-assisted process involving an indirect optical transition.

10.2.3 The Exciton Spin

When we discuss the interaction between an electron and a hole, the definition of the total spin for an exciton is a bit different from the conventional idea of two electrons in a molecule (or a crystal). A hole is a different "particle" from an electron, but, nevertheless, an exchange interaction between the electron and the hole exists, just like for two electrons in a hydrogen molecule.

When an electron absorbs a photon, an electron, for example with spin ↑ is excited to an excited state as shown in Figure 10.2b, leaving behind a hole at the energy level where the electron with up spin ↑ had previously been. This hole has not only a wave vector of $-k$ and an effective mass of $-m^*$ as mentioned in Section 10.2.2, but also is defined to be in a spin down ↓ hole state. The exciton thus obtained (Figure 10.2b) is called a spin singlet exciton, with $S = 0$, since the definition of S for the two-level model shown here is in terms of the two actual electrons that are present,[4] and in this sense the definition for the two actual electrons and for the $S = 0$ exciton are identical. It should also be mentioned that Figure 10.2b does not represent an $S = 0$ eigenstate. To make an eigenstate we must take the antisymmetric combination of the state shown in Figure 10.2b with an electron ↓ and hole ↑ [332]. In contrast, a triplet exciton ($S = 1$) can be represented by two electrons, one in the ground state and the other in an excited state to give a total spin of $S = 1$ (Figure 10.2c).[5] For the triplet state in Figure 10.2c, we define the hole to have a spin ↑ and the resulting state shown here is an eigenstate ($m_s = 1$) for

4) The electric dipole transition does not change the total spin of the ground state which is $S = 0$.
5) The reader should not be confused by having $S = 1$ for the triplet state, since the two spin up electrons are in different energy states.

$S = 1$. We further note that a triplet exciton cannot be recombined by emitting a photon because of the Pauli principle. We call such an exciton, a triplet exciton. A triplet exciton is one type of "dark exciton" (dipole-transition forbidden state).[6] An exchange interaction (> 0) between a hole and an electron works only for $S = 0$ (see Figure 10.2b) and thus the $S = 1$ state in Figure 10.2c has a lower energy than the $S = 0$ state[7] (see also Eq. (10.10) in Section 10.4.1). It should be noted that for the more familiar case of just two electrons, the exchange interaction (< 0) works for the $S = 1$ case and therefore the $S = 1$ state lies lower in energy than the $S = 0$ state.

10.2.4
Localization of Wavefunctions in Real Space

The localization of a wavefunction can be obtained by mixing the Bloch wavefunction labeled by the wave vector k. The equation for determining the mixing of delocalized wavefunctions is called the Bethe–Salpeter equation (Section 10.4.1). The center of mass momentum for an exciton is now a good quantum number in the crystal, while the relative motion of an electron and a hole gives excitonic levels. Thus an exciton is considered to provide a quasi-particle or an elementary excitation with additional freedom, like the plasmon or polariton. By forming an exciton wavefunction, the Hilbert space of the wavefunction for the free particles which describe the electronic states is reduced significantly, and this gives a reduction in the optical absorption for the one-particle spectra. This is known as the oscillator strength sum rule (or f-sum rule). Thus if most of the available oscillator strength for optical absorption is used for the exciton, the spectral intensity for the one-particle transitions is reduced. This situation makes research on excitons for SWNTs more important in the sense that a single-particle excitation has hardly ever been observed in this system in an optical absorption experiment.

The localization length of the exciton in a single-wall carbon nanotube is larger than the diameter of a SWNT but much smaller than the length of a SWNT. This situation gives rise to a predominantly one-dimensional behavior in the optical properties of a SWNT exciton. In a pure 1D exciton, however, the binding energy of the lowest state would be minus infinity. Thus the cylindrical shape of the SWNT is essential for giving a sufficiently large binding energy to the exciton, thus allowing observation of the exciton at room temperature.

6) Spin conversion by a magnetic field could flip a spin and lead to the recombination of the triplet exciton. We will show later another type of dark exciton (E-symmetry exciton).
7) The exchange interaction for the $S = 0$ exciton can be understood as the difference in the interaction energy between two electrons (one at the position of the excited electron and the other at the position of the hole left behind as in Figure 10.2b) and the energy of the $S = 1$ exciton which has no exchange energy (Figure 10.2c).

10.2.5
Uniqueness of the Exciton in Graphite, SWNTs and C_{60}

The electronic structure of a SWNT and of graphite is unique insofar as there are two nonequivalent energy bands near the two hexagonal corners K and K' of the Brillouin zone. We therefore distinguish the regions about K and K' from one another and call them the two valleys of SWNTs and graphite. Although an optical transition occurs vertically in k space, we can consider the electron and the hole in the electron–hole pair to be either in the same valley, or an electron to be in one valley and a hole in the other valley. The latter pair can form an excitonic state in real space, but it never recombines radiatively, since the electron and hole do not have the same k value; we call such a state an E-symmetry exciton (see Section 10.3). An E-exciton is another type of "dark exciton". In addition to the conventional "bright exciton" (an electron–hole pair from the same valley that can recombine radiatively[8]), the coexistence of many different types of excitons is of importance for understanding the optical properties of SWNTs.

In resonance Raman spectra, photoluminescence or resonance Rayleigh scattering, we can observe a signal even from a single SWNT "molecule". In a one-particle picture of optical processes, a strong enhancement of the optical intensities can be understood in terms of the 1D van Hove singularities (vHSs) in the joint density of states connecting the valence and conduction energy bands. In an excitonic picture, an exciton has an energy dispersion as a function of the center of mass wave vector and we expect 1D vHSs in the excitonic density of states from the ground states, where optical absorption becomes strong and this occurs when the center of mass wave vector vanishes. The assignment of the excitation energy to a SWNT with (n, m) indices works well by interpreting the E_{ii}, which is a one-particle picture concept, in terms of the exciton vHS position. This exciton energy position can be modified by electro-chemical doping or by changing the surrounding materials by use of substrates, solutions or wrapping agents (environmental effects) in the space surrounding a SWNT.

In C_{60}, which is a zero-dimensional molecule [6, 333], excitonic behavior is also observed and the binding energy for C_{60} is estimated to be 0.5 eV, which is of the same order of magnitude in energy as the nanotube exciton. This value for C_{60} is obtained by comparing (i) the optical absorption energy (1.55 eV) and (ii) the energy difference observed by photoelectron emission and inverse photoemission spectroscopy (2.3 eV) [334, 335].

The C_{60} and nanotube excitons exhibit fundamental similarities, both systems being π conjugated, both having similar diameters, and both having singularities in their electronic density of states (molecular levels or a narrow energy band width in the C_{60} crystal). On the other hand, the lowest exciton wavefunction is not homogeneous on the C_{60} ball because the electron and hole have their own molecular orbitals with different symmetries. In contrast, in the nanotube exciton, the

8) We will see in Section 10.3 that even within the same valley, one of the two possible exciton types is a dark exciton because of symmetry requirements.

electron and hole have the same symmetry. The lowest exciton wavefunction is homogeneous around the circumferential direction and is localized only along the tube axis direction, because the range of the Coulomb interaction, U, is larger than the tube diameter and smaller than the length of a SWNT. Furthermore, in the case of the C_{60} crystal, the energy band width of the highest occupied molecular orbital (HOMO) and the lowest unoccupied molecular orbital (LUMO) band is much smaller than the Coulomb interaction, while in the case of the nanotube, the energy band width is larger than U. In a SWNT, the motion of the exciton along the nanotube axis gives an energy dispersion for the exciton while the excitons in C_{60} are localized within a molecule. Though we can use similar experimental and theoretical techniques for considering a molecular exciton for C_{60} and for a SWNT, it is nevertheless important to consider the differences in the physics of a 0D and a 1D system when describing excitons in C_{60} and in SWNTs.

10.3 Exciton Symmetry

Group theory discussions tell us that there are four kinds of spin-singlet excitons corresponding to the symmetries, A_1, A_2, $\mathbb{E}$ and $\mathbb{E}^*$ in a SWNT [135], and that only the excitons with A_2 symmetry are optically allowed. We call A_2 excitons "bright excitons" (dipole-transition allowed states) and all other excitons are dark excitons.

10.3.1 The Symmetry of Excitons

Figure 10.3a shows a schematic diagram of the electronic valence and conduction single-particle bands with a given index μ, for general chiral SWNTs [31]. The ir-

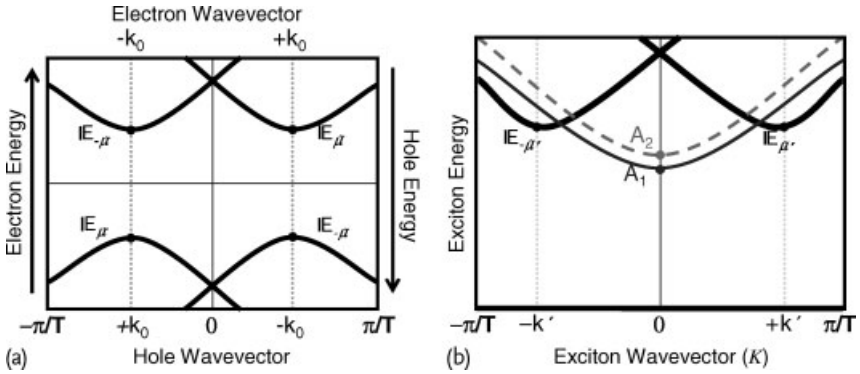

Figure 10.3 (a) Pictorial diagrams for the dispersion of the electronic valence and conduction bands $E(k)$ for chiral (n, m) nanotubes and (b) for their respective excitonic bands. The electron, hole and exciton states at the band edges are indicated by a solid circle and labeled according to the irreducible representation to which they belong [135].

reducible representations of the factor groups of nanotubes are labeled by the angular momentum quantum number μ, which is the index that labels the cutting lines [110]. Here the cutting lines denote the possible k vectors given by the periodic boundary condition around the circumferential direction of a single wall carbon nanotube [110, 336] which can be expressed by $\boldsymbol{k} = \mu \boldsymbol{K}_1 + k\boldsymbol{K}_2/|\boldsymbol{K}_2|$ (where $\mu = 1 - N/2, \ldots, N/2$, and $-\pi/T < k < \pi/T$). Here $\boldsymbol{K}_1$ and $\boldsymbol{K}_2$ are, respectively, the reciprocal lattice vectors along the circumferential and axial directions. N denotes the number of hexagons in the unit cell for SWNTs, and T is the length of the real space unit cell [31]. The electron and hole states at the band-edge are therefore labeled according to their irreducible representations. The exciton wavefunction can be written as a linear combination of products of conduction (electron) and valence (hole) band eigenstates, $\phi_{\mathrm{c}}^{\mu}(\boldsymbol{r}_{\mathrm{e}})$ and $\phi_{\mathrm{v}}^{\mu'*}(\boldsymbol{r}_{\mathrm{h}})$ as [135, 218, 337]

$$\psi(\boldsymbol{r}_{\mathrm{e}}, \boldsymbol{r}_{\mathrm{h}}) = \sum_{\mathrm{v,c},\mu,\mu',k} A_{\mathrm{vc}} \phi_{\mathrm{c}}^{\mu}(\boldsymbol{r}_{\mathrm{e}}) \phi_{\mathrm{v}}^{\mu'*}(\boldsymbol{r}_{\mathrm{h}}), \tag{10.5}$$

where v and c stand for valence- and conduction-band states, respectively. $\phi_{\mathrm{c}}^{\mu}(\boldsymbol{r}_{\mathrm{e}})$ and $\phi_{\mathrm{v}}^{\mu'*}(\boldsymbol{r}_{\mathrm{h}})$ are localized functions in real space which are obtained by taking the summation on k. To obtain an accurate solution for the excitonic eigenfunctions (the A_{vc} coefficients in Eq. (10.5)) and eigenenergies, it is necessary to solve the Bethe–Salpeter equation Section 10.4.1, which includes many-body interactions and considers the mixing by the Coulomb interaction of electron and hole states with all the different wave vectors for all the different bands. The Coulomb interaction depends only on the relative distance between the electron and the hole, and thus the many-body Hamiltonian is invariant under the symmetry operations of the nanotube. Each excitonic eigenstate will then transform as one of the irreducible representations of the space group of the nanotube. In general, the electron–hole interaction will mix states with all wave vectors and all bands, but for moderately small-diameter nanotubes ($d_{\mathrm{t}} < 1.5\,\mathrm{nm}$), the energy separation between singularities in the single-particle JDOS (joint density of states) is fairly large and it is reasonable to consider, as a first approximation, that only the electronic energy sub-bands contributing to a given JDOS singularity E_{ii} will mix to form the excitonic states. Within this approximation, it is possible to employ the usual effective-mass approximation (EMA) and the envelope-function approximation to obtain the exciton eigenfunctions [135, 218, 337]:

$$\psi^{\mathrm{EMA}}(\boldsymbol{r}_{\mathrm{e}}, \boldsymbol{r}_{\mathrm{h}}) = \sum_{\mathrm{v,c}}{}' A_{\mathrm{vc}} \phi_{\mathrm{c}}(\boldsymbol{r}_{\mathrm{e}}) \phi_{\mathrm{v}}^{*}(\boldsymbol{r}_{\mathrm{h}}) F_{\nu}(z_{\mathrm{e}} - z_{\mathrm{h}}) \,. \tag{10.6}$$

The prime in the summation of Eq. (10.6) indicates that only the electron and hole states associated with the JDOS singularity are included. It is important to emphasize that the approximate wavefunctions Ψ^{EMA} have the same symmetries specified by μ as the full wavefunctions Ψ. The envelope function $F_{\nu}(z_{\mathrm{e}} - z_{\mathrm{h}})$ provides an *ad hoc* localization of the exciton in the relative coordinate $z_{\mathrm{e}} - z_{\mathrm{h}}$ along the axis and ν labels the levels in the 1D hydrogenic series given in Section 10.2.1. The envelope functions will be either even ($\nu = 0, 2, 4 \ldots$) or odd ($\nu = 1, 3, 5 \ldots$) upon

the $z \rightarrow -z$ operations.[9] The use of such "hydrogenic" envelope-functions (similar to $f(\boldsymbol{r})$ in Section 10.2.1) serves merely as a physically grounded guess to the ordering in which the different exciton states might appear. From Eq. (10.6), the irreducible representation of the excitonic state $\mathcal{D}(\psi^{\mathrm{EMA}})$ will then be given by the direct product [135, 218, 337]:

$$\mathcal{D}(\psi^{\mathrm{EMA}}) = \mathcal{D}(\phi_{\mathrm{c}}) \otimes \mathcal{D}(\phi_{\mathrm{v}}) \otimes \mathcal{D}(F_{\nu}), \tag{10.7}$$

where $\mathcal{D}(\phi_{\mathrm{c}})$, $\mathcal{D}(\phi_{\mathrm{v}})$ and $\mathcal{D}(F_{\nu})$ are the irreducible representations of the conduction state, valence state and envelope-function F_{ν}, respectively.

As shown in Figure 10.3a, there are two inequivalent electronic bands in chiral tubes,[10] one with the band edge at $k = k_0$ and the other one at $k = -k_0$. In order to evaluate the symmetry of the excitonic states, it is necessary to consider that the Coulomb interaction will mix the two inequivalent states in the conduction band (electrons) with the two inequivalent states in the valence band (holes). These electron and hole states transform as the 1D representations $\mathbb{E}_{\mu}(k_0)$ and $\mathbb{E}_{-\mu}(-k_0)$ of the C_N point group [135],[11] where the conduction and valence band extrema occur at the same $k = k_0$ (or $-k_0$). This situation gives rise to a van Hove singularity (vHS) in the joint density of states (JDOS) [31, 338]. Taking this into consideration, the symmetries of the exciton states associated with the $\nu = 0$ envelope function, which transform as the $A_1(0)$ representation, can be obtained using the direct product in Eq. (10.7):

$$\begin{aligned}\left[\mathbb{E}_{\mu}(k_0) + \mathbb{E}_{-\mu}(-k_0)\right] \otimes \left[\mathbb{E}_{-\mu}(-k_0) + \mathbb{E}_{\mu}(k_0)\right] \otimes A_1(0) \\ = A_1(0) + A_2(0) + \mathbb{E}_{\mu'}(k') + \mathbb{E}_{-\mu'}(-k'),\end{aligned} \tag{10.8}$$

where $k' \sim 2k_0$ and $\mu' = 2\mu$ are the exciton linear momenta and quasi-angular momenta, respectively. Therefore, group theory shows that the set of excitons with the lowest energy is composed of four exciton bands, shown schematically in Figure 10.3. Basically the mixing of two electron and two hole ($\pm\mu$) wave functions generates four exciton states. The mixing of electron and hole states in the same vHSs ($k_{\mathrm{c}} = \pm k_0$, $k_{\mathrm{v}} = \mp k_0$) will give rise to excitonic states, which transform as the A_1 and A_2 irreducible representations of the C_N point group. The excitonic states formed from electrons and holes with $k_{\mathrm{c}} = k_{\mathrm{v}} = \pm k_0$ will transform as the $\mathbb{E}_{\mu'}(k')$ and $\mathbb{E}_{-\mu'}(-k')$ 1D irreducible representations of the C_N point group, with a wave vector k' and an angular momentum quantum number μ'.

The higher-energy exciton states in chiral tubes can be obtained, for instance, by considering the same vHS in the JDOS and higher values of ν. For ν even, the resulting decomposition is the same, since the envelope function also has A_1 symmetry. For odd values of ν, the envelope function will transform as A_2, but that will also leave the decomposition in Eq. (10.8) unchanged. Thus, from the group theory

9) For this symmetry operation, we can use a C_2 axis which is perpendicular to the nanotube axis.

10) The case of achiral nanotubes is given in the problem set for this chapter.

11) Usually E is used to label 2D irreducible representations (IRs) in point groups. In cyclic groups, however, two 1D IRs can be degenerate not by a symmetry in real space, but by time-reversal symmetry. Here these 1D IRs are denoted by $\mathbb{E}$ (see Chapter 6).

point view, both even and odd ν have A_1 and A_2 symmetry excitons. The result is still the same if one now considers higher-energy exciton states derived from higher singularities in the JDOS (for instance, the so-called E_{22} or E_{33} transitions), as long as the angular momentum of the electrons and holes is the same. Therefore, Eq. (10.8) describes the symmetries of all exciton states in chiral nanotubes associated with each E_{ii} transition.

10.3.2
Selection Rules for Optical Absorption

To obtain the selection rules for the optical absorption of the excitonic states, it is necessary to consider that the ground state of the nanotube transforms as a totally symmetric representation (A_1) and that only $K = 0$ excitons can be created (Section 10.2.2). For light polarized parallel to the nanotube axis, the interaction between the electric field and the electric dipole in the nanotube transforms as the A_2 irreducible representation for chiral nanotubes [135]. Therefore, from the four excitons obtained for each envelope function ν, only the A_2 symmetry with $S = 0$ (Section 10.2.3) excitons are optically active for parallel polarized light, and the remaining three states with $S = 1$ are dark states.

Although not related to Raman spectroscopy it is here important to comment that the two-photon absorption experiment [339, 340] represented an important advance for discussing the exciton photophysics of SWNTs. For two-photon excitation experiments, the excitons with A_1 symmetry are accessed, and thus, there will also be one bright exciton for each ν envelope function. The presence of one-photon (two-photon) allowed transitions associated with odd (even) envelope functions result from the presence of two inequivalent vHSs in the first Brillouin zone associated with the two inequivalent carbon atoms in mono-layer graphene. This experiment [339, 340] was considered to prove the excitonic character of the optical levels of SWNTs.

10.4
Exciton Calculations for Carbon Nanotubes

In this section we present some details of the calculations of the excitonic behavior in carbon nanotubes. First a discussion of the Bethe–Salpeter equation is given which is used to calculate the excitonic wavefunctions and their mixing by the Coulomb interaction (Section 10.4.1). Then the energy dispersion of excitons is discussed in Section 10.4.2, while exciton wavefunction calculations are discussed in Section 10.4.3. Finally in Section 10.4.4 the family pattern formation in exciton photophysics is discussed.

10.4.1
Bethe–Salpeter Equation

Here we show how to calculate the exciton energy Ω_n and the wavefunction Ψ^n [186, 311, 319, 321]. Since the exciton wavefunction is localized in real space by a Coulomb interaction, the wave vector of an electron ($\boldsymbol{k}_\mathrm{c}$) or a hole ($\boldsymbol{k}_\mathrm{v}$) is not a good quantum number any more, and thus the exciton wavefunction Ψ_n for the nth exciton energy Ω_n is given by a linear combination of Bloch functions at many $\boldsymbol{k}_\mathrm{c}$ and $\boldsymbol{k}_\mathrm{v}$ wave vectors. The mixing of different wave vectors by the Coulomb interaction is obtained by the so-called Bethe–Salpeter equation [321]

$$\sum_{\boldsymbol{k}_\mathrm{c}\boldsymbol{k}_\mathrm{v}} \left\{ [E(\boldsymbol{k}_\mathrm{c}) - E(\boldsymbol{k}_\mathrm{v})]\delta_{\boldsymbol{k}'_\mathrm{c}\boldsymbol{k}_\mathrm{c}}\delta_{\boldsymbol{k}'_\mathrm{v}\boldsymbol{k}_\mathrm{v}} + K\left(\boldsymbol{k}'_\mathrm{c}\boldsymbol{k}'_\mathrm{v}, \boldsymbol{k}_\mathrm{c}\boldsymbol{k}_\mathrm{v}\right) \right\} \Psi^n(\boldsymbol{k}_\mathrm{c}\boldsymbol{k}_\mathrm{v}) = \Omega_n \Psi^n\left(\boldsymbol{k}'_\mathrm{c}\boldsymbol{k}'_\mathrm{v}\right) , \tag{10.9}$$

where $E(\boldsymbol{k}_\mathrm{c})$ and $E(\boldsymbol{k}_\mathrm{v})$ are the quasi-electron and quasi-hole energies, respectively. Here "quasi-particle" means that we add a Coulomb interaction to the one-particle energy and that the particle has a finite lifetime in an excited state. Equation (10.9) represents simultaneous equations for many $\boldsymbol{k}'_\mathrm{c}$ and $\boldsymbol{k}'_\mathrm{v}$ points.

The mixing term of Eq. (10.9) which we call the kernel, $K(\boldsymbol{k}'_\mathrm{c}\boldsymbol{k}'_\mathrm{v}, \boldsymbol{k}_\mathrm{c}\boldsymbol{k}_\mathrm{v})$ is given by:

$$K\left(\boldsymbol{k}'_\mathrm{c}\boldsymbol{k}'_\mathrm{v}, \boldsymbol{k}_\mathrm{c}\boldsymbol{k}_\mathrm{v}\right) = -K^\mathrm{d}\left(\boldsymbol{k}'_\mathrm{c}\boldsymbol{k}'_\mathrm{v}, \boldsymbol{k}_\mathrm{c}\boldsymbol{k}_\mathrm{v}\right) + 2\delta_S K^\mathrm{x}\left(\boldsymbol{k}'_\mathrm{c}\boldsymbol{k}'_\mathrm{v}, \boldsymbol{k}_\mathrm{c}\boldsymbol{k}_\mathrm{v}\right) , \tag{10.10}$$

with $\delta_S = 1$ for spin singlet states and 0 for spin triplet states (see Section 10.2.3). The direct and exchange interaction kernels K^d and K^x are given by the following integrals [332]:

$$\begin{aligned} K^\mathrm{d}\left(\boldsymbol{k}'_\mathrm{c}\boldsymbol{k}'_\mathrm{v}, \boldsymbol{k}_\mathrm{c}\boldsymbol{k}_\mathrm{v}\right) &\equiv W\left(\boldsymbol{k}'_\mathrm{c}\boldsymbol{k}_\mathrm{c}, \boldsymbol{k}'_\mathrm{v}\boldsymbol{k}_\mathrm{v}\right) \\ &= \int d\boldsymbol{r}' d\boldsymbol{r} \psi^*_{\boldsymbol{k}'_\mathrm{c}}(\boldsymbol{r}')\psi_{\boldsymbol{k}_\mathrm{c}}(\boldsymbol{r}')w(\boldsymbol{r}', \boldsymbol{r})\psi_{\boldsymbol{k}'_\mathrm{v}}(\boldsymbol{r})\psi^*_{\boldsymbol{k}_\mathrm{v}}(\boldsymbol{r}) , \\ K^\mathrm{x}\left(\boldsymbol{k}'_\mathrm{c}\boldsymbol{k}'_\mathrm{v}, \boldsymbol{k}_\mathrm{c}\boldsymbol{k}_\mathrm{v}\right) &= \int d\boldsymbol{r}' d\boldsymbol{r} \psi^*_{\boldsymbol{k}'_\mathrm{c}}(\boldsymbol{r}')\psi_{\boldsymbol{k}'_\mathrm{v}}(\boldsymbol{r}')v(\boldsymbol{r}', \boldsymbol{r})\psi_{\boldsymbol{k}_\mathrm{c}}(\boldsymbol{r})\psi^*_{\boldsymbol{k}_\mathrm{v}}(\boldsymbol{r}) , \end{aligned} \tag{10.11}$$

where w and v are the screened and bare Coulomb potentials, respectively, and ψ is the quasi-particle wavefunction as discussed below.

The quasi-particle energies are the sum of the single-particle energy ($\epsilon(\boldsymbol{k})$) and self-energy ($\Sigma(\boldsymbol{k})$),

$$E(\boldsymbol{k}_\mathrm{i}) = \epsilon(\boldsymbol{k}_\mathrm{i}) + \Sigma(\boldsymbol{k}_\mathrm{i}) , \quad (i = \mathrm{c}, \mathrm{v}) , \tag{10.12}$$

where $\Sigma(\boldsymbol{k})$ is expressed by:

$$\begin{aligned} \Sigma(\boldsymbol{k}_\mathrm{c}) &= -\sum_{\boldsymbol{q}} W(\boldsymbol{k}_\mathrm{c}(\boldsymbol{k}+\boldsymbol{q})_\mathrm{v}, (\boldsymbol{k}+\boldsymbol{q})_\mathrm{v}\boldsymbol{k}_\mathrm{c}) , \\ \Sigma(\boldsymbol{k}_\mathrm{v}) &= -\sum_{\boldsymbol{q}} W(\boldsymbol{k}_\mathrm{v}(\boldsymbol{k}+\boldsymbol{q})_\mathrm{v}, (\boldsymbol{k}+\boldsymbol{q})_\mathrm{v}\boldsymbol{k}_\mathrm{v}) . \end{aligned} \tag{10.13}$$

In order to obtain the kernel and self-energy, the single-particle Bloch wavefunction $\psi_{\boldsymbol{k}}(\boldsymbol{r})$ and screening potential w are obtained by either a first principles calculation [321] or an extended tight-binding wavefunction and a random phase approximation (RPA) calculation [186]. In the RPA calculation, the static screened Coulomb interaction is expressed by:

$$w = \frac{v}{\kappa\epsilon(\boldsymbol{q})} , \tag{10.14}$$

with a static dielectric constant κ and the dielectric function $\epsilon(\boldsymbol{q}) = 1 + v(\boldsymbol{q})\Pi(\boldsymbol{q})$. By calculating the polarization function $\Pi(\boldsymbol{q})$ and the Fourier transformation of the unscreened Coulomb potential $v(\boldsymbol{q})$, we get information, which is sufficient for describing the exciton energy and wavefunction [186, 319]. For one-dimensional materials, the Ohno potential is commonly used for the unscreened Coulomb potential $v(q)$ for π orbitals [324]

$$v(|\boldsymbol{R}_{u's'} - \boldsymbol{R}_{0s}|) = \frac{U}{\sqrt{\left((4\pi\epsilon_0/e^2)\,U|\boldsymbol{R}_{us} - \boldsymbol{R}_{0s'}|\right)^2 + 1}} , \tag{10.15}$$

where U is the energy cost to place two electrons on a single site ($|\boldsymbol{R}_{us} - \boldsymbol{R}_{0s'}| = 0$) and this energy cost is taken as $U \equiv U_{\pi_a\pi_a\pi_a\pi_a} = 11.3$eV for π orbitals [324].

10.4.2
Exciton Energy Dispersion

For an electron–hole pair, we introduce wave vectors $\boldsymbol{K}$ for the exciton center of mass and $\boldsymbol{k}$ for the relative motion,

$$\boldsymbol{K} = (\boldsymbol{k}_{\rm c} - \boldsymbol{k}_{\rm v})/2 , \quad \boldsymbol{k} = \boldsymbol{k}_{\rm c} + \boldsymbol{k}_{\rm v} . \tag{10.16}$$

The Bethe–Salpeter equation (Eq. (10.9)) is then rewritten in terms of $\boldsymbol{K}$ and $\boldsymbol{k}$. Since the Coulomb interaction is related to the relative coordinate of an electron and a hole, the center-of-mass motion $\boldsymbol{K}$ can be treated as a good quantum number.[12)] Thus the exciton energy is given by an energy dispersion as a function of $\boldsymbol{K}$.

In Figure 10.4, we show the two-dimensional Brillouin zone (2D BZ) of graphite and the cutting lines for a (6,5) single-wall carbon nanotube. Since optical transitions occur around the K or K' points in the 2D BZ, we can expect four possible combinations of an electron and hole pair as is discussed in Section 10.3.1 and as is shown in Figure 10.4. The excitons in a SWNT can then be classified according to their $2\boldsymbol{K}$ values. If both the electron ($\boldsymbol{k}_{\rm c}$) and hole ($\boldsymbol{k}_{\rm v}$) wave vectors are from the K (or K') region, then $2\boldsymbol{K} = \boldsymbol{k}_{\rm c} - \boldsymbol{k}_{\rm v}$ lies in the Γ region and the corresponding exciton is an $A_{1,2}$ symmetry exciton. If an electron is from the K region and a hole is from the K' region, their $2\boldsymbol{K}$ lies in the K region and this exciton is an $\mathbb{E}$ symmetry exciton. If an electron is from the K' region and a hole is from the K region, their $2\boldsymbol{K}$ lies in the K' region and this exciton is an $\mathbb{E}^*$ symmetry exciton.

12) Strictly speaking, when we consider the screening effect of an exciton by other electrons, $\boldsymbol{K}$ is no longer a good quantum number.

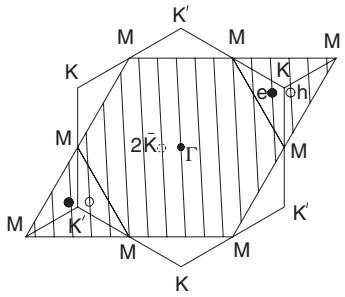

Figure 10.4 The three inequivalent regions in the 2D Brillouin zone of graphite. The cutting lines (Section 10.3.1) for a (6,5) SWNT are shown. The electron–hole pairs and the corresponding center-of-mass momentum $2\boldsymbol{K} = \boldsymbol{k}_c - \boldsymbol{k}_v$ for an $A_{1,2}$ exciton of the (6,5) SWNT are indicated. The electron–hole pair where the electron and hole lie on the second and first cutting lines relative to the K point and the electron–hole pair where the electron and hole lie on the first and second cutting lines relative to the K' point correspond to an E_{12} exciton with the center-of-mass momentum $2\boldsymbol{K}$ on the first cutting line relative to the Γ point [186].

As we discussed in the symmetry section (Section 10.3.1), the exciton wavefunction should be described by an irreducible representation of the group of the wave vector for a SWNT. For A excitons, the electron–hole pair wavefunction $|\boldsymbol{k}_c, \boldsymbol{k}_v\rangle = |\boldsymbol{k}, \boldsymbol{K}\rangle$ with the electron and hole from the K region, and $|-\boldsymbol{k}_v, -\boldsymbol{k}_c\rangle = |-\boldsymbol{k}, \boldsymbol{K}\rangle$ with the electron and hole from the K' region have the same magnitude for $\boldsymbol{K}$. Thus, we can recombine these two electron–hole pairs to get

$$A_{2,1} = |\boldsymbol{k}, \pm, \boldsymbol{K}\rangle = \frac{1}{\sqrt{2}}(|\boldsymbol{k}, \boldsymbol{K}\rangle \pm |-\boldsymbol{k}, \boldsymbol{K}\rangle) \,. \tag{10.17}$$

Here $|\boldsymbol{k}, +, \boldsymbol{K}\rangle$ and $|\boldsymbol{k}, -, \boldsymbol{K}\rangle$ are antisymmetric (A_2) and symmetric (A_1), respectively, under the C_2 rotation around the axis perpendicular to the nanotube axis.[13)]

10.4.3
Exciton Wavefunctions

In this section we discuss mainly the calculated results relevant to bright excitons [186]. In Figure 10.5, we plot the energy dispersion of $E_{ii}(A_j)$ ($i = 1, 2$; $j = 1, 2$) excitons with spin $S = 0, 1$ for a (6,5) SWNT, where E_{ii} denotes the energy separation of the ith valence band to the ith conduction band. We use the same notation of E_{ii} for the exciton [229], too, for simplicity. The exciton with the largest energy dispersion shows a parabolic energy dispersion relation which reflects the free particle behavior of an exciton with a mass. For the A_1 exciton, $S = 0$ and $S = 1$ are degenerate, since the exchange interaction vanishes by symmetry. Figure 10.5d gives the excitation energy levels for $K = 0$ $E_{11}(A^{\nu})$ states. We note that for the spin $S = 0$ states, $E_{11}(A_2^0)$ has a somewhat larger energy than $E_{11}(A_1^0)$. This

13) It might be confusing that $+$ ($-$) corresponds to antisymmetric (symmetric) wavefunctions. But it is a correct statement.

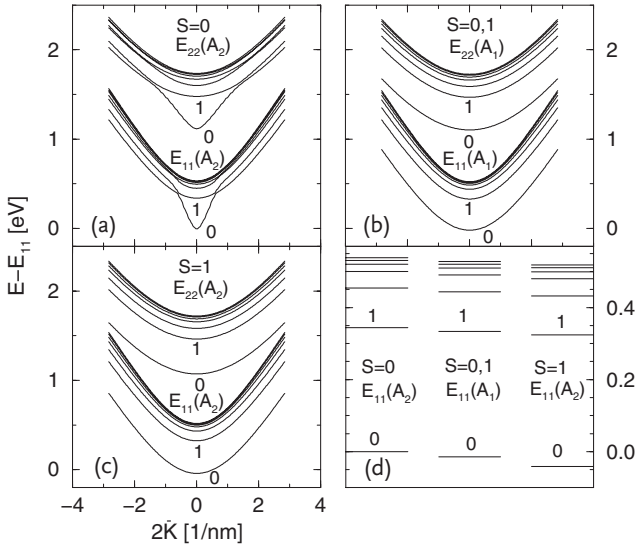

Figure 10.5 The excitation energy dispersions for (a) $E_{11}(A_2)$ ($S = 0$) and $E_{22}(A_2)$ ($S = 0$), (b) $E_{11}(A_1)$ ($S = 0, 1$) and $E_{22}(A_1)$ ($S = 0, 1$), and (c) $E_{11}(A_2)$ ($S = 1$) and $E_{22}(A_2)$ ($S = 1$) excitons for a (6,5) SWNT. The excitation energy levels for $\boldsymbol{K} = 0$ excitons are also shown in (d) [186].

means that the bright A_2 exciton is not the lowest energy state [341]. The Coulomb energy $K^{\mathrm{d}}(\boldsymbol{k}', -\boldsymbol{k}; \pm, \boldsymbol{K})$, which is the energy for an inter-valley scattering process, thus has a one order of magnitude smaller energy than the corresponding energy for an intravalley scattering process, $K^{d}(\boldsymbol{k}', \boldsymbol{k}; \pm, \boldsymbol{K})$. Therefore, the energy difference between $E_{11}(A_2^0)$ and $E_{11}(A_1^0)$ (for $S = 0$) is predicted to be quite small (about 12meV in Figure 10.5d). Moreover, in Figure 10.5d the triplet $E_{11}(A_2^0)$ state lies about 35meV below the singlet $E_{11}(A_2^0)$ state. The energy difference between the triplet and singlet $E_{11}(A_2)$ states is determined by the exchange Coulomb interaction, $K^{\mathrm{x}}(\boldsymbol{k}', \boldsymbol{k}; \boldsymbol{K})$ (see Eq. (10.11)), which is about one order of magnitude smaller than the direct Coulomb interaction $K^{\mathrm{d}}(\boldsymbol{k}', \boldsymbol{k}; \boldsymbol{K})$ in SWNTs. The energy difference between the singlet $E_{11}(A_2^0)$ state and the $E_{11}(A_1^0)$ state, and the energy difference between the singlet and triplet $E_{11}(A_2^0)$ states are consistent for different calculations [320, 325].

Hereafter, we will mainly discuss the singlet bright exciton $E_{ii}(A_2^0)$ states with $K = 0$. In Figure 10.6 we show the exciton wavefunctions along the nanotube axis of an (8,0) SWNT for several of the $E_{22}(A_2^\nu)$ states with lower excitation energies and with $\nu = 0, 1$, and 2, namely (a) $E_{22}(A_2^0)$, (b) $E_{22}(A_2^1)$ and (c) $E_{22}(A_2^2)$ [186]. Because of the orthogonalization of the wavefunctions, we can see wavefunctions with 0, 1, 2 nodes in Figure 10.6a–c, respectively. The localization of the wavefunction for $E_{22}(A_2^0)$ for the (8,0) SWNT is around 1 nm at full width half maximum intensity. The localization length increases with increasing energy and with increasing nanotube diameter, reflecting the dimensional change from 1D to 2D.

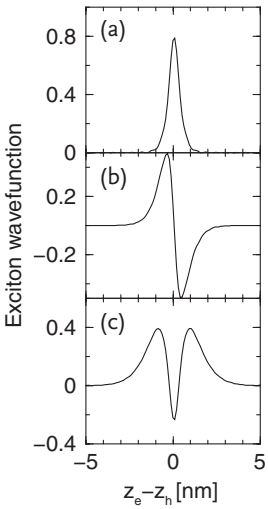

Figure 10.6 The magnitude of the exciton wavefunctions along the nanotube axis of an (8,0) SWNT for the states: (a) $E_{22}(A_2^0)$, (b) $E_{22}(A_2^1)$ and (c) $E_{22}(A_2^2)$ [186].

In a SWNT or in graphite, there are two sublattices, A and B. For $E_{22}(A_2^0)$ and $E_{22}(A_2^2)$, the wavefunctions have a similar amplitude for the A and B sublattices, while for $E_{22}(A_2^1)$, the amplitude of the wavefunction of the electron and hole occupies one of the two sublattice exclusively. The latter behavior of the wavefunction (that the amplitude of the wavefunction can exist only on one sublattice) can be seen for localized edge states. Thus we expect an interesting behavior to occur when the exciton becomes localized at the end of a SWNT.

The $E_{22}(A_2^0)$ and $E_{22}(A_2^2)$ excitons are symmetric and the $E_{22}(A_2^1)$ exciton is antisymmetric upon reflection about the z axis. It then follows that the $E_{22}(A_2^0)$ and $E_{22}(A_2^2)$ excitons are bright and the $E_{22}(A_2^1)$ exciton is dark with respect to linearly polarized light parallel to the z axis.[14] In the two-photon absorption experiments, the $E_{22}(A_2^2)$ exciton becomes bright [339]. For an achiral (armchair or zigzag) SWNT, exciton wavefunctions are either even or odd functions of z because of the inversion center in these SWNTs. Thus, we use A_{2u} or A_{2g} to label $E_{22}(A_2^1)$, or $E_{22}(A_2^0)$ (and $E_{22}(A_2^2)$), respectively, for achiral SWNTs [218].

The localized exciton wavefunction is constructed by mixing many k states in which the mixing coefficients are determined by the Bethe–Salpeter equation (Eq. (10.9)). We found above that the envelope functions for the three wave functions given in Figure 10.6 can, respectively, be fitted to a Gaussian (e^{-Cz^2}, ze^{-Cz^2}, $(Az^2 - B)e^{-Cz^2}$). The mixing coefficients (Fourier transformation) are also localized in k space around one particle k points for a given E_{ii}, and this localization is described by the wavefunction full-width at half maximum magnitude ℓ_k.

14) An important fact in discussing this statement is that the A_2 wavefunction itself has a minus sign under a C_2 rotation or z reflection. Thus an even function of z becomes a dipole-allowed exciton state.

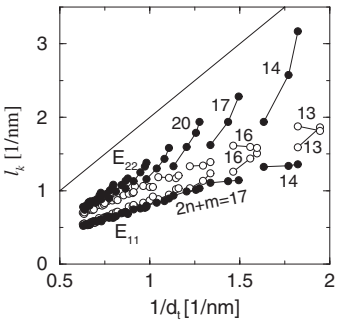

Figure 10.7 The half width ℓ_k of the wave functions in 1D k space for the $E_{11}(A_2^0)$ and $E_{22}(A_2^0)$ states. The cutting line spacing $2/d_t$ is shown by the solid line for comparison. Open and filled circles, respectively, denote SI and SII SWNTs, where SI and SII denote the semiconductor tube type in SWNTs. Integers denote the $2n+m$ values for individual SWNT families [186].

In Figure 10.7, we plot ℓ_k in the 1D k space for the bright exciton states, $E_{11}(A_2^0)$ and $E_{22}(A_2^0)$, and for all SWNTs with diameters (d_t) in the range of 0.5 nm $< d_t <$ 1.6 nm. In Figure 10.7, we also plot the cutting line spacing $2/d_t$ by the solid line. An important message here is that ℓ_k is smaller than $2/d_t$ for all SWNTs. This result indicates that one cutting line is sufficient to describe individual $E_{ii}(A)$ states. Consequently, the difficulty in calculating the Bethe–Salpeter equation is reduced significantly for the case of carbon nanotubes. For the higher energy states, $E_{ii}(A_2^\nu)$ states with $\nu = 1, 2, \cdots$, have ℓ_k values that are smaller than that for $E_{ii}(A_2^0)$, since the wavefunctions for $E_{ii}(A_2^\nu)$ are more delocalized in real space. Generally, we can say that the ith cutting line is sufficient to describe the $E_{ii}(A)$, $E_{ii}(\mathbb{E})$ and $E_{ii}(\mathbb{E}^*)$ states[15] and that the ith and $(i+1)$th cutting lines are sufficient to describe the $E_{ii+1}(A)$ and $E_{i+1i}(A)$ states. Since metallic SWNTs (M-SWNTs) have smaller ℓ_k values than semiconducting SWNTs (S-SWNTs), the above conclusion is also valid for M-SWNTs.

The assumption, that we consider only one cutting line, is valid so long as the range of the Coulomb interaction is larger than the diameter d_t of a SWNT. For a typical nanotube diameter ($0.5 < d_t < 2.0$ nm), the Coulomb interaction is sufficiently strong for all carbon atoms along the circumferential direction, so that the wavefunction for the E_{ii} exciton becomes constant around the circumferential direction, which is the physical reason why we need only one cutting line. When the diameter is sufficiently large compared to the range of the Coulomb interaction (more than 5 nm), the exciton wavefunction is no longer constant around the circumferential direction (two-dimensional exciton), and then we need to use the kernel from neighboring cutting lines in the Bethe–Salpeter equation.

It is important to mention that for the wavefunction for the $E_{ii+1}(A)$ exciton, which is excited by perpendicularly polarized light (see Section 9.2.3), we must consider two cutting lines (i and $i+1$) for the wavefunction (see Figure 10.4),

15) For the $\mathbb{E}$ exciton, the $\pm i$ states are considered for the electron and the hole.

because of the dipole selection rule. In fact, the calculated exciton has an anisotropy around the circumferential direction in the sense that the electron and hole exist with respect to each other at opposite sides of the nanotube. Since the induced depolarization field [238] cancels the optical field, there is a significant upshift of the energy position of $E_{ii+1}(A)$ relative to the $E_{ii}(A)$ excitonic transition [238, 315]. This upshift in energy has been observed in PL experiments [311, 312] and can also be observed in maps of RRS spectra.

10.4.4
Family Patterns in Exciton Photophysics

Based on resonance Raman spectroscopy studies, it is found that the optical transition energies E_{ii} when plotted against tube diameter exhibit family patterns related to the $2n + m =$ constant families (see Section 9.3). These family patterns are also observed in two-dimensional photoluminescence (PL) plots [180]. The reason why we get family patterns is that (n, m) SWNTs within the same $2n + m =$constant family have diameters similar to one another and that the E_{ii} values are generally inversely proportional to the nanotube diameter. The small change of the E_{ii} values within the same family is due to the trigonal warping effect of the electronic dispersion around the K (and K') point [229]. The trigonal warping effect and the θ-dependent lattice distorion gives a chirality dependence both for the one-particle energy position at a van Hove singular k point, and the corresponding effective mass. The change of the effective mass for the various SWNTs belonging to the same $(2n + m)$ family is important for determining the exciton binding energy and self-energy for each SWNT.

The energy spread in a family becomes large as the diameter decreases and becomes less than 1 nm. In this case, the simple tight-binding calculation in which we consider only π electrons is not sufficient to reproduce the E_{ii} energy positions. To address this problem, the extended tight-binding (ETB) calculation has been developed (Section 10.1) in which the curvature effect is taken into account by the mixing of the π orbitals with the σ and $2s$ orbitals of carbon. When we then add the density functional form of the many-body effect to the ETB results, we can reproduce nicely the experimental results for the dependence of the E_{ii} on diameter and chiral angle [299, 342].

In Figure 10.8 we plot the exciton Kataura plot for the $E_{11}^S(A_2^0)$ and $E_{22}^S(A_2^0)$ states for S-SWNTs and the $E_{11}^M(A_2^0)$ states for M-SWNTs. Open and filled circles are for Type I and II (SI and SII) SWNTs, respectively, and crossed circles are for M-SWNTs. SI and SII SWNTs are defined by $\mathrm{mod}(2n + m, 3) = 1$ and $\mathrm{mod}(2n + m, 3) = 2$, respectively [336], where mod is the modulus function of integers. The E_{ii} values are the sum of the ETB one-particle energies, the self-energy Σ and the exciton binding energy E_{bd}. We note that a large family spread appears in Figure 10.8, which is consistent with both calculations [182, 299] and experiments [180, 183].

In Figure 10.9, we plot separately each contribution to the ETB (extended tight-binding) transition energy E_{11}, the self-energy Σ of the quasi-particle, and the ex-

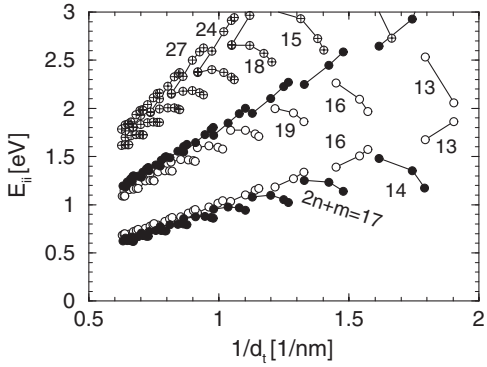

Figure 10.8 The excitation energy Kataura plot based on the extended tight-binding model for $E_{11}^S(A_2^0)$ and $E_{22}^S(A_2^0)$ for S-SWNTs and $E_{11}^M(A_2^0)$ for M-SWNTs. Open and filled circles are for SI and SII SWNTs, respectively, and crossed circles are for M-SWNTs [186].

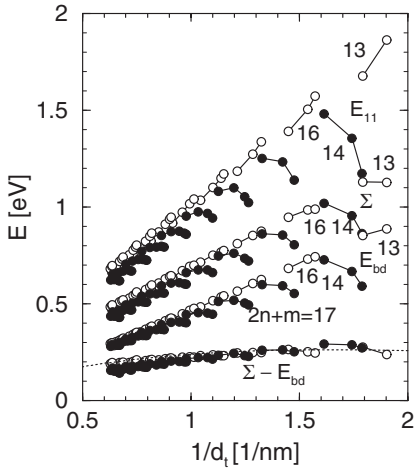

Figure 10.9 The excitation energy E_{11}^S, self-energy Σ, binding energy E_{bd} and energy corrections $\Sigma - E_{bd}$ based on the ETB model for $E_{11}(A_2^0)$ bright exciton states. Open and filled circles are, respectively, for SI and SII SWNTs. The dashed line is calculated by Eq. (10.18) with $p = 1$ [186].

citon binding energy E_{bd}. We also plot $\Sigma - E_{bd}$ in the same figure [186]. It is seen that although both Σ and E_{bd} tend to increase the family spread, the two terms almost cancel each other regarding the family spread. This near cancellation leads to a weak chirality dependence, showing that the net energy correction ($\Sigma - E_{bd}$) to the single-particle energy depends predominantly on the SWNT diameter. Thus, we conclude that the large family spread that is observed in E_{11} originates predominantly from the trigonal warping effect and the θ-dependent lattice distortion in the single-particle spectra. It is known that the logarithmic correction due to the effect of the Coulomb interaction on the dispersion of 2D graphite is not canceled by

the exciton binding energy and this effect leads to a logarithmic energy correction $E^{\log}$ given by [181, 299]

$$E^{\log} = 0.55(2p/3d_t)\log[3/(2p/3d_t)]\,, \tag{10.18}$$

which is the rationale for the logarithmic term is the empirical Eq. (9.10). In Figure 10.9, we plot $E^{\log}$ with $p = 1$ as a dashed line, thus showing that the energy correction $\Sigma - E_{bd}$ follows this logarithmic behavior well. This good agreement for $\Sigma - E_{bd}$ explains why the ETB model works well in considering excitonic and other many-body effects occurring in SWNT photophysics.

10.5
Exciton Size Effect: the Importance of Dielectric Screening

The E_{ii} values are now understood in terms of the bright exciton energy within the framework of a tight-binding calculation which includes curvature optimization [182, 329] and many-body effects [37–39, 186, 343]. The assignments of E_{ii} for SWNTs over a large region of both diameter ($0.7 < d_t < 3.8$ nm) and E_{ii} (1.2–2.7 eV) values and for a variety of surrounding materials are now available [20, 317], thus making it possible to accurately determine the effect of the general dielectric constant κ on E_{ii}. By "general" we mean that κ comprises the screening from both the tube and from the environment. A d_t-dependent effective κ value for the exciton calculation is needed to reproduce the experimental E_{ii} values consistently. This dependence is important for the physics of quasi and truly one-dimensional materials generally and can be used in interpreting optical experiments and environment effects for such materials.

10.5.1
Coulomb Interaction by the 2*s* and σ Electrons

Figure 10.10 shows a map of experimental E_{ii} values (black dots) [189, 317] from a SWNT sample grown by the water-assisted ("super-growth") chemical vapor deposition method [33, 281]. The resulting data for the E_{ii} transition energies are plotted as a function of the radial breathing mode frequencies ω_{RBM}, as obtained by resonance Raman spectroscopy (RRS) [189, 317, 318]. In Figure 10.10, the experimental values of E_{ii} vs. ω_{RBM} for the "super-growth" sample E_{ii}^{exp} are compared with the calculated bright exciton energies E_{ii}^{cal} (open circles and stars), obtained with the dielectric screening constant $\kappa = 1$. Although E_{ii}^{cal} includes SWNT curvature and many-body effects [186], clearly the E_{ii}^{exp} values are red shifted when compared with theory, and the red shift depends on both ω_{RBM} (i. e., on d_t) and on the optical energy levels (i in E_{ii}).

The E_{ii} values can be renormalized in the calculation by explicitly considering the dielectric constant κ in the Coulomb potential energy given by Eq. (10.14) [344]. Here, κ represents the screening of the e–h (electron–hole) pair by core (1*s*) and σ electrons (κ_{tube}) and by the surrounding materials (κ_{env}), while $\varepsilon(q)$ explicitly gives

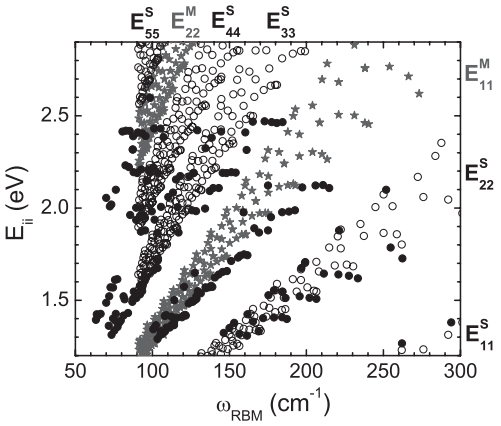

Figure 10.10 Black dots show E_{ii}^{exp} vs. ω_{RBM} results obtained from resonance Raman spectra taken from a "super-growth" SWNT sample [189, 317]. The black open circles (semiconducting; S-SWNTs) and the dark gray stars (metallic; M-SWNTs) give E_{ii}^{cal} calculated for the bright exciton with dielectric constant $\kappa = 1$ [186]. Along the x axis, E_{ii}^{cal} are translated using the relation $\omega_{\text{RBM}} = 227/d_{\text{t}}$ [189]. Due to limited computer time availability, only E_{ii} for tubes with $d_{\text{t}} < 2.5\,\text{nm}$ (i. e., $\omega_{\text{RBM}} > 91\,\text{cm}^{-1}$) have been calculated. Transition energies E_{ii}^{S} ($i = 1$ to 5) denote semiconducting SWNTs and E_{ii}^{M} ($i = 1, 2$) denote metallic SWNTs [190].

the polarization function for π-electrons calculated within the random phase approximation (RPA) [186, 324, 345]. To fully account for the observed energy-dependent E_{ii} redshift, the total κ values are fitted to minimize $E_{ii}^{\text{exp}} - E_{ii}^{\text{cal}}$. The bullets in Figure 10.11 show the fitted κ values as a function of p/d_{t}, which reproduce each experimental E_{ii} value for the assigned (n, m) SWNTs for the "super-growth" SWNT sample. The stars stand for a different SWNT sample, named "alcohol-assisted" SWNTs [346], and these differences are due to different environmental screening (κ_{env}), as discussed later in Section 10.5.2. The integer p corresponds to the distance ratio of the cutting lines from the K point, where $p = 1, 2, 3, 4$ and 5 are for E_{11}^{S}, E_{22}^{S}, E_{11}^{M}, E_{33}^{S}, and E_{44}^{S}, respectively [20]. Consideration of the p/d_{t} ratio allows us to compare the κ values of SWNTs with different d_{t} and different E_{ii} using the same plot. As seen in Figure 10.11, the κ values increase with increasing p/d_{t} for different E_{ii} values. The κ values for E_{33}^{S} and E_{44}^{S} (Figure 10.11b) appear over a smaller κ region than those for E_{11}^{S} and E_{22}^{S} (Figure 10.11a).

The data points in Figure 10.11 can be fit with the empirical relation [190]

$$\kappa = C_{\kappa}\left(\frac{p}{d_{\text{t}}}\right)^{\alpha}, \tag{10.19}$$

where the exponent $\alpha = 1.7$ was found to work for all E_{ii}^{exp}, but different C_{κ} parameters were needed for different samples to reflect the differences in their environmental conditions [190]. For E_{11}^{S}, E_{22}^{S} and E_{11}^{M}, the value $C_{\kappa} = 0.75$ was obtained for the "super-growth" SWNTs and $C_{\kappa} = 1.02$ for the "alcohol-assisted" SWNTs (dashed and dotted curves in Figure 10.11a, respectively), and these differences

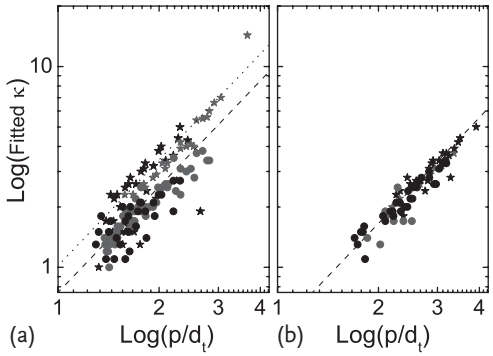

Figure 10.11 The calculated κ values, which are fitted to the experimental E_{ii} values from the "super-growth" (bullets) [317] and "alcohol-assisted" (stars) [287] samples. (a) E_{22}^S (black) and E_{11}^M (dark gray). The dashed and dotted curves are given by Eq. (10.19) with $C_\kappa = 0.75$ and 1.02, respectively. (b) E_{33}^S (black) and E_{44}^S (dark gray). The dashed curves are for Eq. (10.19) with $C_\kappa = 0.49$ [190].

can be understood by κ_{env}. The E_{33}^S and E_{44}^S are fitted using $C_\kappa = 0.49$ for both samples, as shown by the dashed line in Figure 10.11b.

Qualitatively, the origin of the diameter dependence of the dielectric constant presented by Eq. (10.19) consists of: (1) the exciton size and (2) the amount of electric field "feeling" the dielectric constant of the surrounding material. These two factors are connected and the development of an electromagnetic model is needed to fully rationalize this equation. Interestingly, the similarity between the κ values found for E_{22}^S and E_{11}^M shows that the difference between metallic and semiconducting tubes is satisfactorily taken into account by using the RPA in calculating $\varepsilon(q)$ [343]. Also interesting is the different κ behavior that is observed for higher energy levels ($p > 3$), where C_κ is smaller than for E_{ii} with $p \leq 3$, and in this regime κ is independent of the sample environment. Two pictures can be given: (1) the more localized exciton wavefunction (a larger exciton binding energy) for E_{33}^S and E_{44}^S compared with E_{11}^M and E_{22}^S, leads to smaller κ values and a lack of a κ_{env} dependence of the wavefunctions for the E_{33}^S and E_{44}^S excitons; (2) the stronger tube screening (κ_{tube}) leads to an independence regarding κ_{env} and, consequently, leads to a smaller effective κ.

10.5.2
The Effect of the Environmental Dielectric Constant κ_{env} Term

Figure 10.12 shows a comparison between the E_{ii}^{exp} from the "super-growth" SWNT sample (bullets) [317] and from the "alcohol-assisted" SWNT samples (open circles) [287]. From Figure 10.12, we see that besides the changes in ω_{RBM}, as discussed in Section 9.1.2, the E_{ii}^{exp} values from the "alcohol-assisted" SWNTs are generally red shifted with respect to those from the "super-growth" SWNTs. Assuming that κ_{tube} does not change from sample to sample for a particular type of SWNT sample, since the structure of a given (n, m) tube should be the same, these results

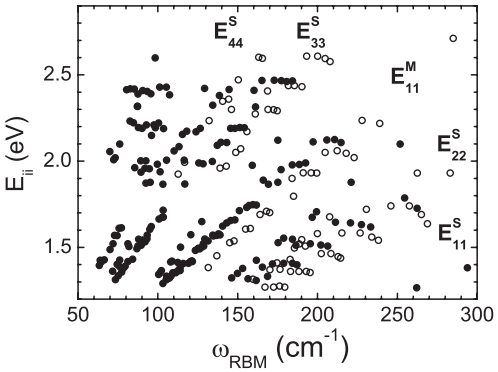

Figure 10.12 E_{ii}^{exp} vs. ω_{RBM} results obtained for the "super-growth" (bullets) and the "alcohol assisted" (open circles) SWNT samples [190].

indicate that the "alcohol-assisted" SWNTs are surrounded by a larger κ_{env} value, than the "super growth" sample, thus increasing the effective κ and decreasing E_{ii} [190].

Looking at Figure 10.11 we can observe the difference in the κ values resulting from fitting the E_{ii}^{exp} to the "super-growth" (bullets) in comparison to "alcohol-assisted" (stars) SWNT samples. For E_{22}^S and E_{11}^M (Figure 10.11a), we see a clear difference for κ up to $p = 3$ when comparing the two samples. However, for E_{33}^S and E_{44}^S (Figure 10.11b), no difference in κ between the two samples can be seen. This means that the electric field of the E_{33}^S and E_{44}^S excitons does not extend much outside the SWNT volume, in contrast to the E_{22}^S and E_{11}^M excitons for which the κ_{env} effect is significant. Since the effect of κ_{env} is relatively small for energies above E_{11}^M, it is still possible to assign the (n, m) values from E_{33}^S and E_{44}^S even if the dielectric constant of the environment is not known, and even though the E_{33}^S and E_{44}^S values are seen within a large density of dots in the Kataura plot.

10.5.3
Further Theoretical Considerations about Screening

The dielectric constant for the materials surrounding the SWNTs cannot be directly used in calculations or in interpreting data, since the electric field exists not only in the surrounding materials but also in the SWNTs themselves. In the calculations shown in Figure 10.13, the dielectric constant κ is treated as a parameter which is used in the Ohno potential and $\Delta E_{ii}^S \equiv \Delta E_{ii}^S(\kappa = 2) - \Delta E_{ii}^S(\kappa = 3) > 0$ is plotted as a function of $1/d_t$. In this figure, we can see the $(2n + m)$ family pattern for type I (S1, $\text{mod}(2n + m, 3) = 1$) and type II (S2, $\text{mod}(2n + m, 3) = 2$) semiconducting SWNTs for ΔE_{11}^S and ΔE_{22}^S. This predicted behavior is consistent with recent experimental results [347, 348].

In Figure 10.14, we plot E_{ii}^S for a (6,5) SWNT as a function of (a) $1/\kappa$ or (b) κ with (solid lines) and without (dashed lines) including the electron screening ef-

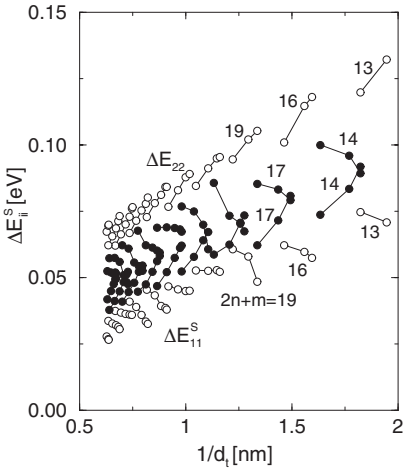

Figure 10.13 Calculated shifts in the E_{11}^S and E_{22}^S transition energies due to changing κ from 3 to 2. Open and filled circles are, respectively, for S1 and S2 type semiconducting SWNTs [186].

fect for the E_{11}^S and E_{22}^S states for a (6,5) SWNT. It is seen that without considering the electron screening effect, E_{ii}^S is approximately linearly dependent on $1/\kappa$. The screening effect will bend the line, reducing the energy shift, especially for the small κ region, for example, $\kappa < 2$. The bending effect arises from the fact that the screening effect by the environment generally provides a dielectric constant, independent of the wave vector $\boldsymbol{q}$, while the effect of the dielectric function $\epsilon(0, q)$ on the E_{ii}^S transition energies resulting from the electron screening effect is a function of q [319]. In Figure 10.14a, we also show the exciton binding energy vs. $1/\kappa$. It is seen that for both E_{11} and E_{22} states, the binding energy approximately scales as

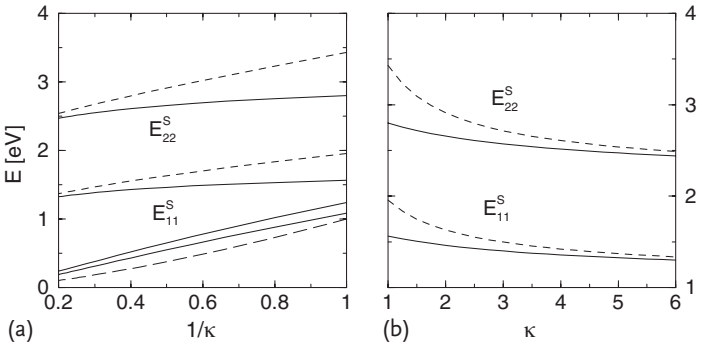

Figure 10.14 The transition energy dependence on κ for states E_{11}^S and E_{22}^S for a (6,5) SWNT. Solid and dashed lines, respectively, do or do not consider the π electron screening effect. (a) Excitation energy vs. $1/\kappa$. The three curves below E_{11} give the $1/\kappa$-dependent exciton binding energies for E_{22}^S and E_{11}^S, and the function $E = (1/\kappa)^{1.4}$ from top to bottom, respectively. (b) Excitation energy vs. κ for E_{11}^S and E_{22}^S [186].

$(1/\kappa)^{1.4}$. This scaling parameter α can be used for estimating the exciton binding energy E_{bd} as:

$$E_{\mathrm{bd}} \propto d_{\mathrm{t}}^{\alpha-2} m^{\alpha-1} \kappa^{-\alpha} , \tag{10.20}$$

where m is the effective mass of the electron or hole [324]. The concept of scaling is useful for explaining the observed family patterns and diameter dependence of the E_{ii}. The diameter dependence on κ is relevant to this scaling rule, which is still not well understood [219].

10.6 Summary

In this chapter we have discussed the exciton science in carbon nanotubes. This discussion starts after introducing the importance of $\sigma - \pi$ hybridization in the curved graphene sheet of carbon nanotubes. Excitons are important in semiconductors generally, but they are especially important in nanomaterials, where the spatial confinement enhances the overlap between optically excited electrons and holes, thus enhancing the exciton binding energy. We here discuss the physics of exciton levels, wave vectors, spin, symmetry aspects, selection rules, energies, wavefunctions, that is, all the aspects important for achieving an accurate description of the optical levels in nanotubes. However, to achieve experimental accuracy, a treatment of the dielectric screening also has to be considered.

The diameter-dependent dielectric constants following Eq. (10.19) reproduce the measured E_{ii} values well for a large region of energy (1.2–2.7 eV) and tube diameter (0.7–3.8 nm). The present treatment for κ is sufficiently accurate for assigning both the $2n + m$ family numbers and the (n, m) SWNTs belonging to each family for different SWNT samples. All the observed E_{ii} vs. (n, m) values are now theoretically described within their experimental precision, considering use of the extended tight-binding model along with many-body corrections plus a diameter-dependent dielectric constant κ (Eq. (10.19)). The empirical Eq. (10.19) is not yet fully understood, and theoretical modeling considering the role of the exciton size is still needed. The results presented here are also consistent with the empirical methodology of Eq. (9.10) [287], and therefore provide justification for this approach.

Problems

[10-1] When the planar sp^2 bond is bent in the circumferential direction by an angle θ which is on the order of $\theta = 0.1$ rad, we expect a large curvature effect. What is the corresponding tube diameter?

[10-2] The curvature effect can be understood by the Slater–Koster method in which the transfer matrix element for π–π orbitals is mixed with σ–σ or-

bitals. Show how the matrix element is modified as a function of θ in Problem 10-1.

[10-3] Applying the wavefunction of Eq. (10.2) to Eq. (10.1), obtain the differential equations for g and f.

[10-4] Solve the one-dimensional hydrogen Schrödinger equation. In particular show that the lowest energy is minus infinity. Obtain the corresponding wavefunction.

[10-5] Solve the two-dimensional hydrogen Schrödinger equation. In this case, we have an angular momentum within a plane. Obtain the energies.

[10-6] When the potential is spherical in three dimensions, the potential is given as a function of r. In this case, show that the angular part of the wavefunction for the Hamiltonian with a spherical potential is given by the spherical harmonics, $Y_{lm}(\theta, \varphi)$.

[10-7] Obtain the differential equation on r for a hydrogen atom with angular momentum ℓ, and solve this equation for the bound states of the hydrogen atom.

[10-8] Explain what are the direct and indirect energy gaps by showing some example in the case of semiconductors. In the case of an indirect energy gap, explain that the exciton cannot only emit a photon.

[10-9] When electron–electron interaction U exists between two electrons, explain that the interaction modifies electronic states mainly near the Fermi energy. In particular, why are the electrons at the bottom of the energy band not affected much by the Coulomb interaction. Consider the two cases that (1) $U \gg W$ (W: energy band width), and (2) $W \gg U$.

[10-10] Explain qualitatively what you expect for the energy dispersion $E(k)$, if electrons have a finite lifetime in the presence of some interaction.

[10-11] When the wavefunction is spatially localized, the wavefunction is expressed by a linear combination of Bloch wavefunctions with many k values. In order to understand this, calculate the Fourier transform of a Gaussian function $f(x) = \exp(-x^2/a^2)$.

[10-12] The spin functions of an electron with $s_z = 1/2$ and $-1/2$ are denoted by α and β, respectively. When we define the spin of a hole by $s_z = -1/2$ and $1/2$, respectively, for the states which are originally occupied by an electron with $s_z = 1/2$ and $-1/2$ and denoted by β_{h} and α_{h}, obtain the total spin function of a singlet ($S = 0$) and a triplet ($S = 1$) exciton.

[10-13] When we consider the electric-dipole transition which does not depend on spin, explain that the $S = 1$, $S_z = -1, 0, 1$ exciton states are all dark exciton states.

[10-14] In the presence of a Coulomb interaction, an energy difference between the $S = 1$ and $S = 0$ states of two electrons appears, which is known as the exchange energy. Explain the physical meaning of the exchange energy in terms of the Pauli exclusion principle, the Hartree–Fock approximation, and the spin of two electrons. Why are the $S = 1$ states lower in energy than the $S = 0$ states?

[10-15] Explain the reason why the $S = 0$ exciton does not relax quickly to the lower energy $S = 1$ states.

[10-16] Derive Eq. (10.8) for achiral SWNTs and draw schematics similar to those of Figure 10.3 for both zigzag and armchair tubes.

[10-17] Illustrate figures similar to Figure 10.4 for the E_{11} exciton levels for A_1, A_2 and E symmetries. What happens for E_{22} or E_{12} excitons? Note that two configurations are coupled when explaining A_1 and A_2 excitons (see Eq. (10.17)).

[10-18] Why does the plus sign in Eq. (10.17) correspond to the antisymmetric A_2 exciton? Discuss how the wavefunctions of the valence and conduction bands change by a C_2 rotation.

[10-19] Compare Eq. (10.18) with the logarithmic part of Eq. (9.10) and discuss the results.

[10-20] Show that the effective mass for the E_{33}^S or E_{44}^S exciton is larger than that for E_{11}^S or E_{22}^S.

[10-21] By considering the $1s$ energy of a hydrogen atom, show that the exciton binding energy becomes large when the effective mass of the electron and hole is large. From this, show that the exciton binding energy of the E_{33}^S or E_{44}^S exciton is larger than that for the E_{11}^S or E_{22}^S exciton.

[10-22] When the dielectric constant of the surrounding material κ_{env} is large, which exciton feels κ_{env} more, E_{11}^S or E_{33}^S? Explain by illustrating the electric field for these excitons.

[10-23] In a $2n + m =$ const. family, which SWNTs have a larger effective mass, near armchair SWNTs or near zigzag SWNTs?

[10-24] Using the fact that the distance of the K point from the Γ point in the direction perpendicular to the cutting line is $K\Gamma = (2n + m)/3$, illustrate the cutting lines for the E_{11}^S to E_{44}^S transitions for S1 and S2 SWNTs in the two-dimensional Brillouin zone.

[10-25] For E_{11}^S, which semiconducting type has a larger effective mass, S1 or S2? How about for E_{22}^S?